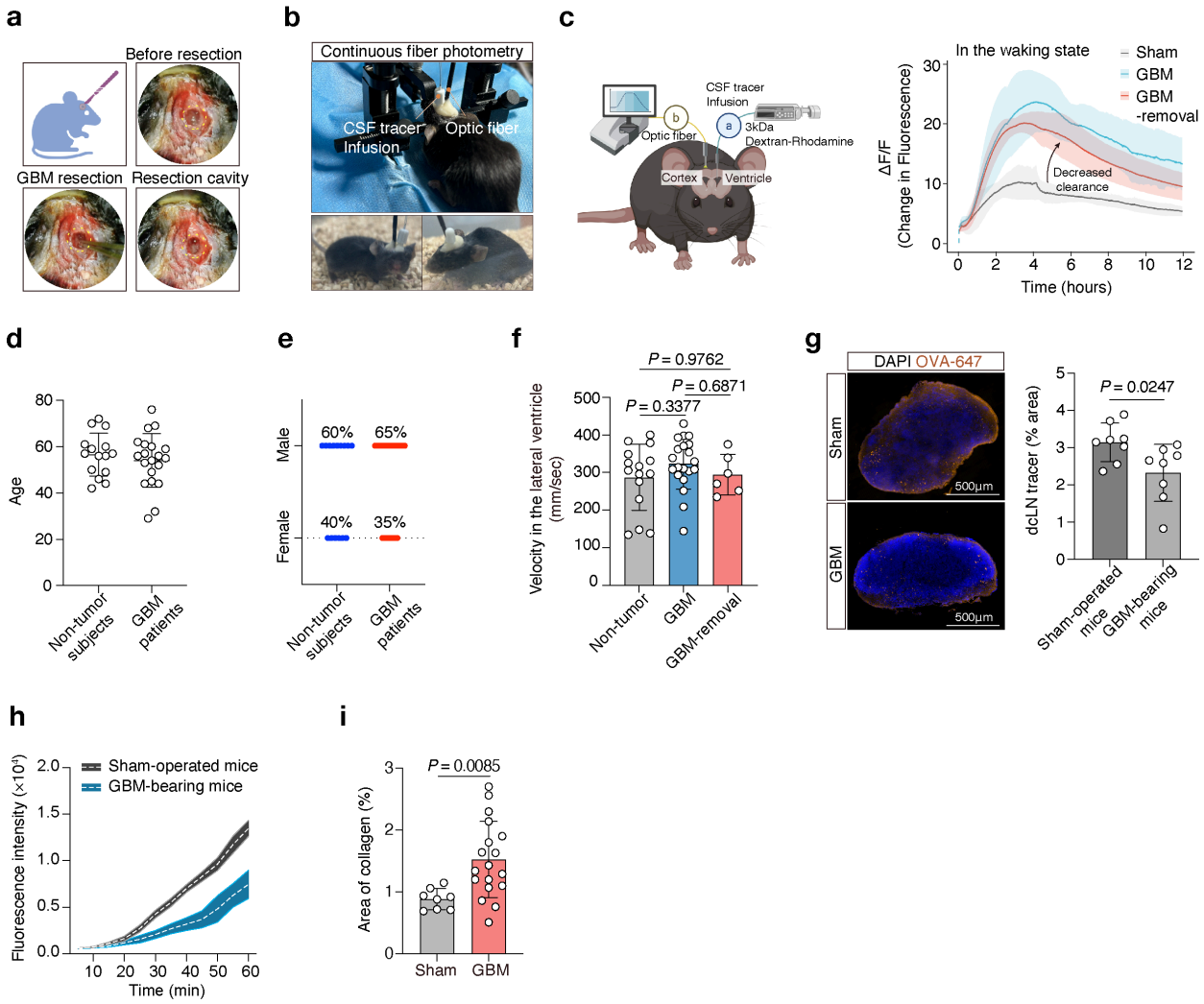

Extended Data Fig. 1 | Dynamics of cerebrospinal fluid in GBM-bearing mice.

a, Schematic of tumor resection in the orthotopic GBM tumor-bearing mouse model under microscopy.

b, Schematic of lateral ventricle catheter implantation and tracer (FITC-dextran, 3 kDa) injection methodology, with tracer administration and monitoring performed in awake mice.

c, Dynamic fluorescence signal changes of CSF tracers in the cortical region for Sham, GBM, and GBM-removal groups (n = 3 mice per group). Figure created with BioRender.com.

d–e, Age and sex distribution of non-tumor controls (reference) and GBM patients included in phase-contrast MRI (PC-MRI) analysis.

f, Bar graphs showing lateral ventricle flow velocity changes in non-tumor control individuals (mean ± s.d., n = 15), GBM patients (mean ± s.d., n = 20), and postoperative GBM patients (mean ± s.d., n = 6).

g, Left: Representative fluorescence images of deep cervical lymph nodes in Sham and GBM tumor-bearing mouse models after CSF injection with the tracer Ovalbumin-AF647. Scale bar, 500 μm. Right: Bar graphs showing the fluorescent coverage area of deep cervical lymph nodes (mean ± s.d., n = 8 mice per group).

h, Fluorescence signal changes in venous blood samples within 60 minutes after CSF injection of the tracer (Ovalbumin-AF647) in Sham and GBM tumor-bearing mouse models (n = 3 mice per group).

i, Bar graphs showing the area of leptomeningeal I/III collagen fibers ($COL1A1^+/COL3A1^+$) in Sham (mean ± s.d., n = 8 mice) and GBM tumor-bearing mouse models (mean ± s.d., n = 18 mice).

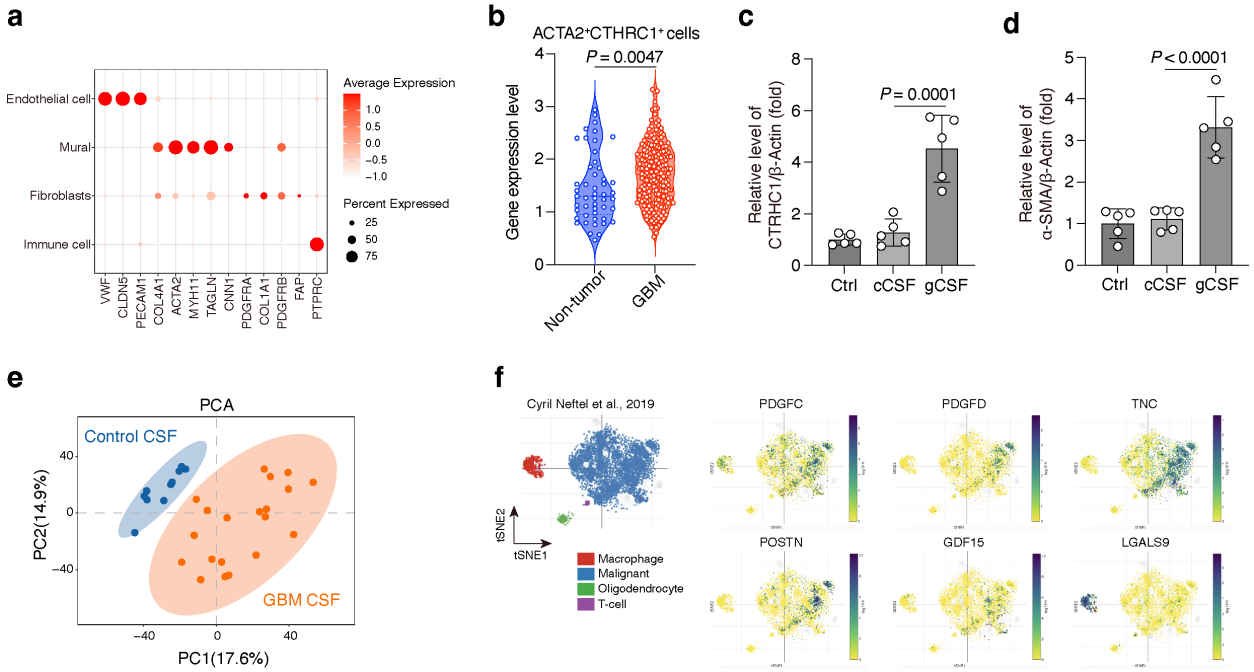

Extended Data Fig. 2 | $CTHRC1^+$α-SMA^+ leptomeningeal fibroblasts and GBM-CSF derived secretory proteins.

a, Annotation information for cell clusters in single-cell data from leptomeningeal tissues of non-tumor controls (n = 3) and GBM patients (n = 3).

b, Features of $CTHRC1^+$α-SMA^+ pathological fibroblasts in leptomeningeal fibroblasts of non-tumor control individuals and GBM patients. The y-axis represents the mean gene expression of the target cell cluster (mean ± s.d.). Each point in the violin plot represents a single $CTHRC1^+$α-SMA^+ pathological fibroblast.

c–d, Protein level changes of CTHRC and α-SMA in HEbF cells treated with cerebrospinal fluid from non-tumor control individuals (cCSF) or GBM patients (gCSF) (mean ± s.d., n = 5 per group).

e, Principal component analysis (PCA) of proteomics data from CSF samples of GBM patients (n = 20) and non-tumor control patients (n = 10).

f, t-SNE plot showing the expression of genes corresponding to differentially upregulated secretory proteins in CSF samples of GBM patients vs. non-tumor controls in GBM tumor tissues.

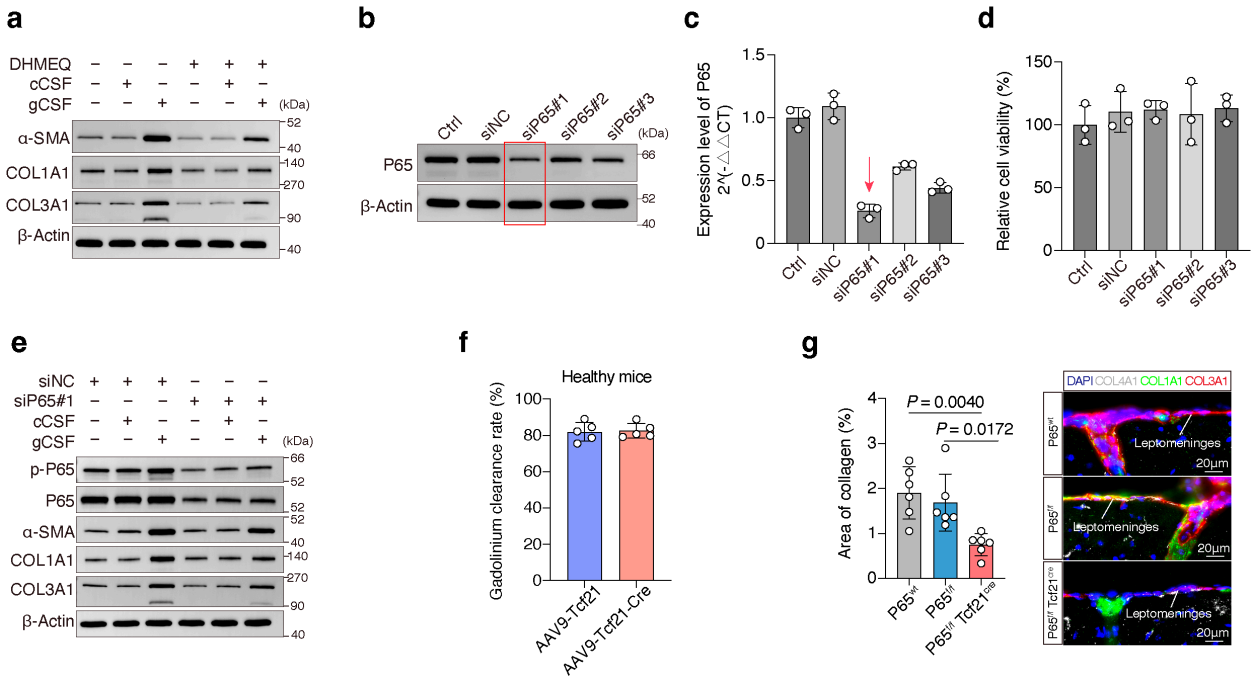

Extended Data Fig. 3 | NF-κB/P65 signaling in leptomeningeal fibroblasts regulates CSF clearance and collagen deposition.

a, Protein expression levels of α-SMA, COL1A1, and COL3A1 in hPLMFs treated with cCSF or gCSF following DHMEQ (a selective P65 inhibitor) intervention.

b-c, Protein expression and RNA levels of P65 in hPLMFs after siRNA transfection (mean ± s.d., n = 3 per group).

d, Cell viability of hPLMFs after siP65 transfection (mean ± s.d., n = 3 per group).

e, Protein expression levels of phosphorylated P65, total P65, α-SMA, COL1A1, and COL3A1 in hPLMFs treated with cCSF or gCSF after P65 gene silencing via siRNA.

f, Bar graphs showing the impact of P65 knockout in leptomeningeal fibroblasts on gadobutrol clearance rate in healthy mouse CSF (mean ± s.d., n = 5 per group).

g, Left: Bar graphs showing the area of I/III collagen fibers in the leptomeninges of GBM tumor-bearing mice in the $P65^{wt}$, $P65^{f/f}$, and $P65^{f/f}Tcf^{Cre}$ groups (mean ± s.d., n = 6 per group). Right:

Representative images of I/III collagen fibers in the leptomeninges of these groups. Scale bar, 20 μm.

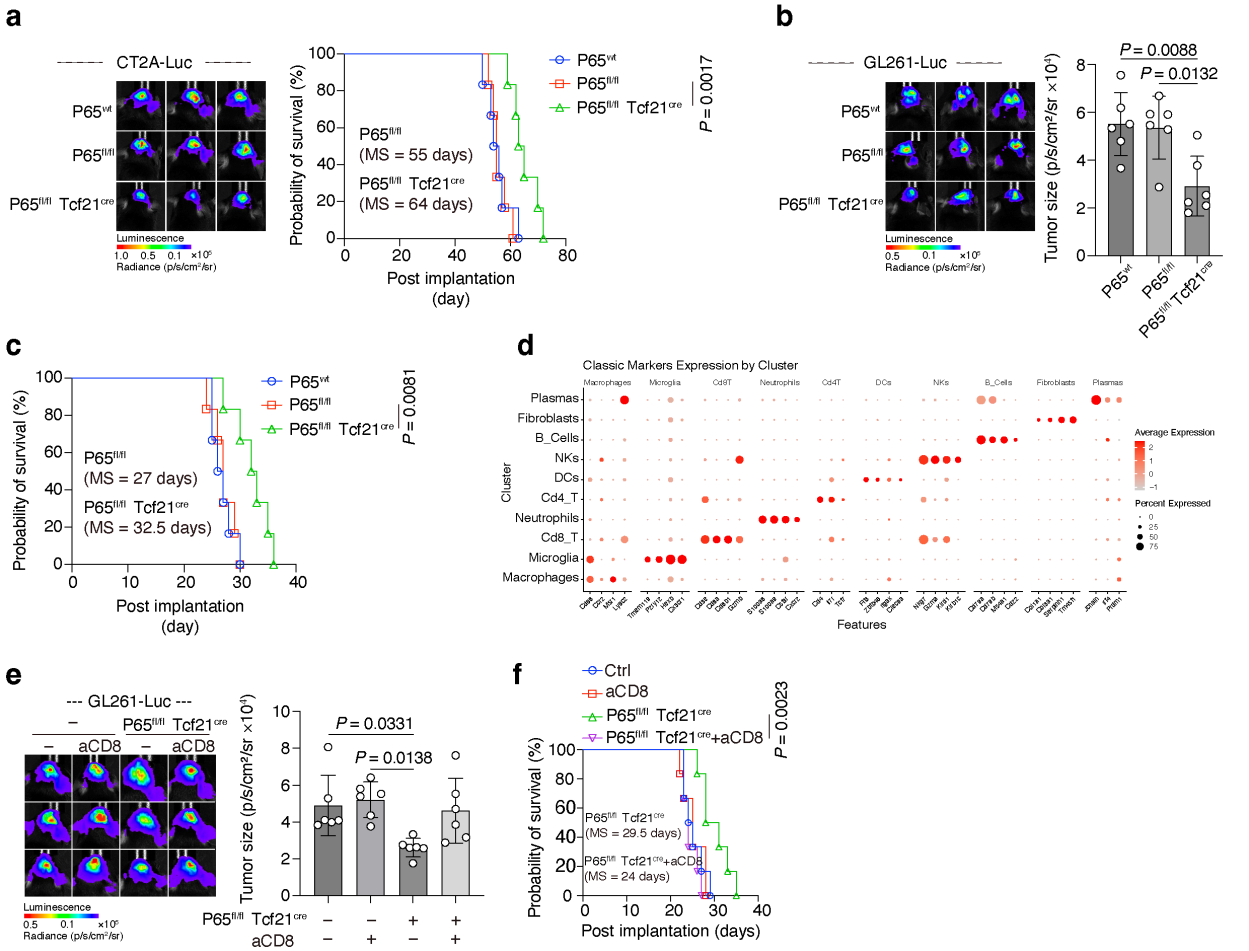

Extended Data Fig. 4 | NF-κB/P65 signaling in leptomeningeal fibroblasts regulates GBM progression via CSF clearance and CD8⁺ T cell immunity.

a, Left: Representative bioluminescence imaging images of CT2A-Luc tumor-bearing mice in the $P65^{wt}$, $P65^{f/f}$, and $P65^{f/f}Tcf^{Cre}$ groups. Right: Survival curves of CT2A-Luc tumor-bearing mice in each group (n = 6 per group, Log-rank test).

b, Left: Representative bioluminescence imaging images of GL261-Luc tumor-bearing mice in the $P65^{wt}$, $P65^{f/f}$, and $P65^{f/f}Tcf^{Cre}$ groups. Right: Bar graphs showing tumor burden size in each group (mean ± s.d., n = 6 per group).

c, Survival curves of GL261-Luc tumor-bearing mice in the $P65^{wt}$, $P65^{f/f}$, and $P65^{f/f}Tcf^{Cre}$ groups (n = 6 per group, Log-rank test).

d, Single-cell RNA sequencing data of $CD45^+$ cells in tumor tissues of CT2A-Luc tumor-bearing mice in the $P65^{f/f}$, and $P65^{f/f}Tcf^{Cre}$ groups, showing the division and annotation of 10 immune cell subpopulations and biomarkers.

e, Left: Representative bioluminescence imaging images of GL261-Luc tumor-bearing mice in the $P65^{f/f}$, and $P65^{f/f}Tcf^{Cre}$ groups treated with IgG isotype or anti-CD8α neutralizing antibodies. Right: Bar graphs showing tumor burden size in GL261-Luc tumor-bearing mice (mean ± s.d., n = 6 per group).

f, Survival curves showing the therapeutic effects of IgG isotype and anti-CD8α neutralizing antibodies in $P65^{f/f}$, and $P65^{f/f}Tcf^{Cre}$ mice (GL261-Luc model) (n = 6 per group, Log-rank test).

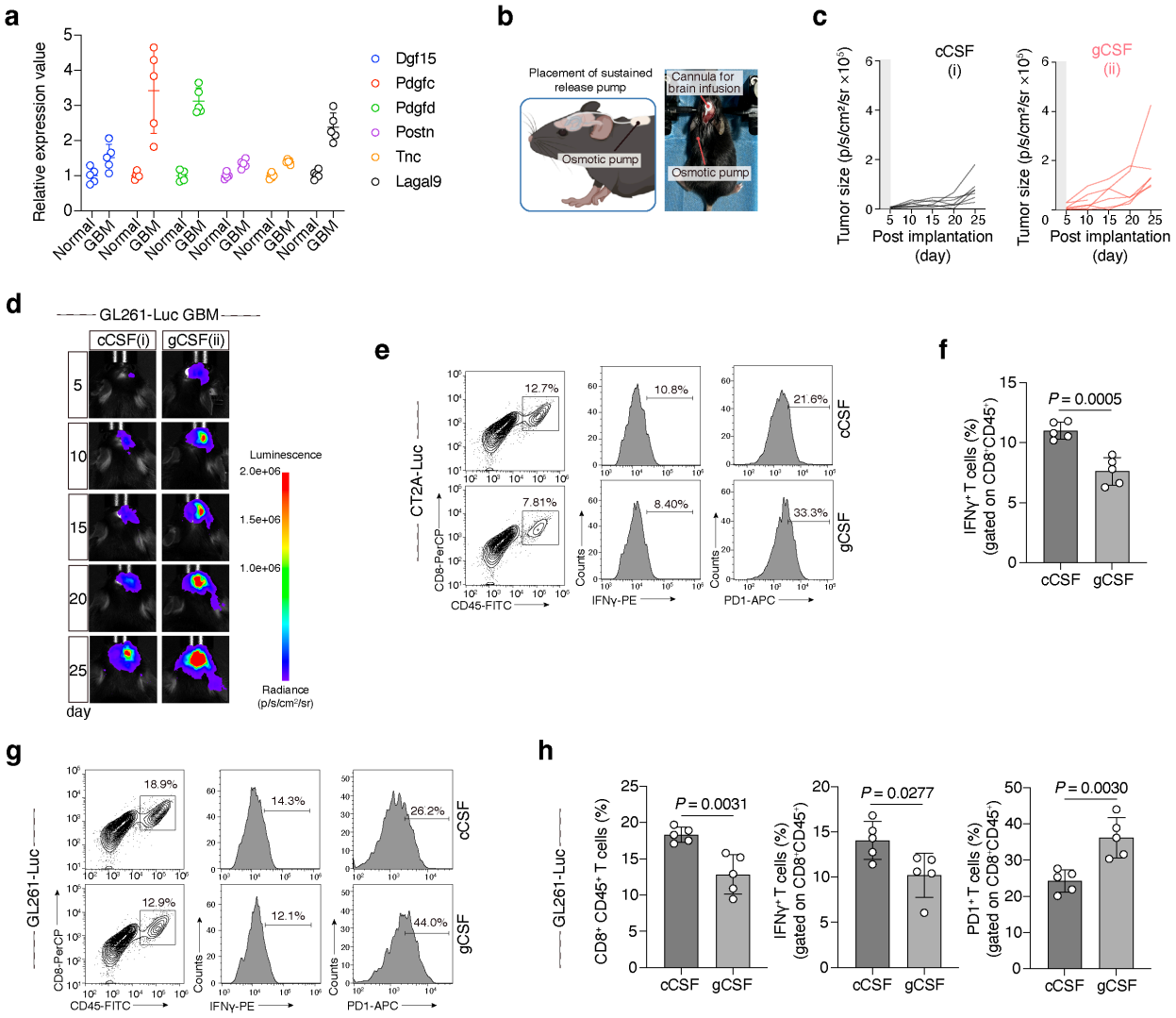

Extended Data Fig. 5 | Impaired CSF clearance drives GBM progression via CD8⁺ T cell exhaustion.

a, Expression levels of representative secretory proteins (Dgf15, PDGFC, PDGFD, TNC, POSTN, and LGALS9) in the CSF of CT2A-Luc tumor-bearing mice (mean ± s.d., n = 5 per group).

b, Schematic of the placement and implantation of osmotic pumps and injection cannulas in the CSF replacement experiment. Figure created with BioRender.com.

c, Tumor burden size in GL261-Luc tumor-bearing mice of the cCSF and gCSF groups (mean ± s.d., n = 7 per group).

d, Representative bioluminescence imaging images of GL261-Luc tumor-bearing mice in the cCSF and gCSF groups.

e, Representative flow cytometry images of $CD45^+CD8^+$ cells, IFN-γ^+ cells (gated on $CD45^+CD8^+$), and $PD1^+$ cells (gated on $CD45^+CD8^+$) in tumor tissues of CT2A-Luc tumor-bearing mice in the cCSF and gCSF groups.

f, Bar graphs showing the proportion of IFN-γ^+ cells (gated on $CD45^+CD8^+$) in tumor tissues of CT2A-Luc tumor-bearing mice (mean ± s.d., n = 5 per group).

g, Representative flow cytometry images of $CD45^+CD8^+$ cells, IFN-γ^+ cells (gated on $CD45^+CD8^+$), and $PD1^+$ cells (gated on $CD45^+CD8^+$) in tumor tissues of GL261-Luc tumor-bearing mice in the cCSF and gCSF groups.

h, Bar graphs showing the proportions of $CD45^+CD8^+$ cells, IFN-γ^+ cells (gated on $CD45^+CD8^+$), and $PD1^+$ cells (gated on $CD45^+CD8^+$) in tumor tissues of GL261-Luc tumor-bearing mice (mean ± s.d., n = 5 per group).

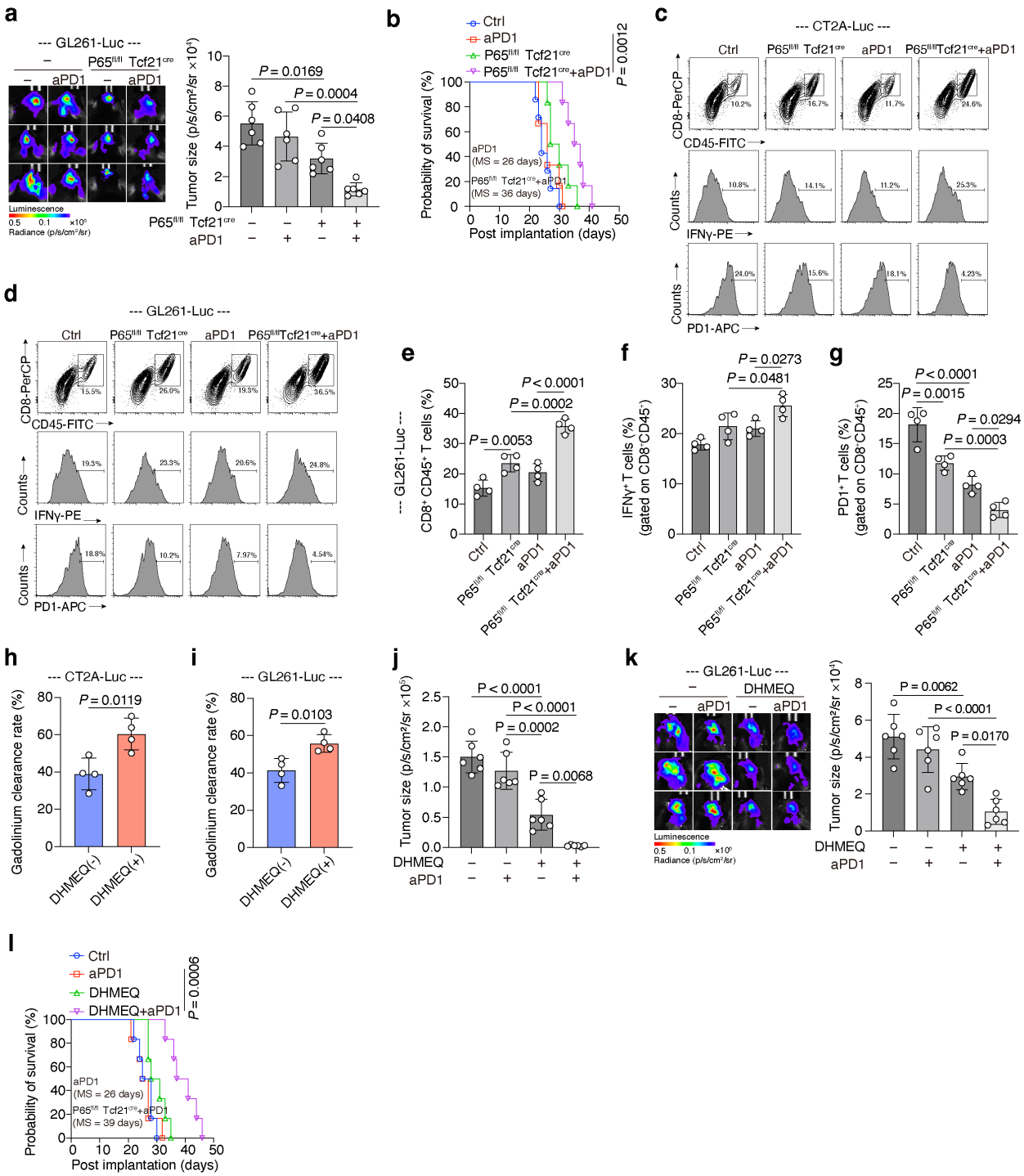

Extended Data Fig. 6 | Combined P65 inhibition and anti-PD-1 therapy synergistically enhances GBM treatment via improved CSF clearance and CD8⁺ T cell function.

a, Left: Representative bioluminescence imaging images of GL261-Luc tumor-bearing mice in the Ctrl, aPD1, P65$^{f/f}$Tcf^{Cre}, and aPD1 + P65$^{f/f}$Tcf^{Cre} groups. Right: Bar graphs showing tumor burden in these mice (mean ± s.d., n = 6 per group).

b, Survival curves of GL261-Luc tumor-bearing mice in the Ctrl, aPD1, $P65^{f/f}Tcf^{Cre}$, and aPD1 + $P65^{f/f}Tcf^{Cre}$ groups. (n = 6 per group, Log-rank test).

c–d, Representative flow cytometry images of $CD45^+CD8^+$ cells, IFN-γ^+ cells (gated on $CD45^+CD8^+$), and $PD1^+$ cells (gated on $CD45^+CD8^+$) in tumor tissues of CT2A/GL261-Luc tumor-bearing mice in the control (Ctrl), anti-PD1 monotherapy (aPD1), $P65^{f/f}Tcf^{Cre}$, and aPD1 + $P65^{f/f}Tcf^{Cre}$ groups.

e–g, Bar graphs showing the proportions of $CD45^+CD8^+$, IFN-γ^+ cells (gated on $CD45^+CD8^+$), and $PD1^+$ cells (gated on $CD45^+CD8^+$) in tumor tissues of GL261-Luc tumor-bearing mice in the control (Ctrl), $P65^{f/f}Tcf^{Cre}$, anti-PD1 monotherapy (aPD1), and aPD1 + $P65^{f/f}Tcf^{Cre}$ groups (mean ± s.d., n = 4 per group).

h–i, Bar graphs showing CSF clearance rate in CT2A-Luc and GL261-Luc tumor-bearing mice after DHMEQ treatment (mean ± s.d., n = 4 per group).

j, Bar graphs showing tumor burden of CT2A-Luc tumor-bearing mice in the Ctrl, DHMEQ, aPD1, and aPD1 + DHMEQ groups. (mean ± s.d., n = 6 per group).

k, Left: Representative bioluminescence imaging images of GL261-Luc tumor-bearing mice in the control (Ctrl), DHMEQ monotherapy, anti-PD1 monotherapy (aPD1), and aPD1 + DHMEQ groups. Right: Tumor burden in each group (mean ± s.d., n = 6 per group).

l, Survival curves of GL261-Luc tumor-bearing mice in the control (Ctrl), DHMEQ monotherapy, anti-PD1 monotherapy (aPD1), and aPD1 + DHMEQ groups (n = 6 per group, Log-rank test).